ELSEVIER

Contents lists available at ScienceDirect

Earth and Planetary Science Letters

journal homepage: www.elsevier.com/locate/epsl



Tracing magmatic genesis and evolution through single zircon crystals from successive supereruptions from the Socorro Caldera Complex, USA



Sean P. Gaynor a,b,*, Tyson M. Smith c,d, Urs Schaltegger a

- ^a Department of Earth Sciences, University of Geneva, 1205, Geneva, Switzerland
- ^b Department of Geosciences, Princeton University, Princeton, NJ, 08544, United States of America
- ^c United States Geological Survey, Denver, CO, United States of America
- d Department of Marine, Earth and Atmospheric Sciences, North Carolina State University, Raleigh, NC, 27695, United States of America

ARTICLE INFO

Article history: Received 30 November 2022 Received in revised form 11 May 2023 Accepted 21 May 2023 Available online 7 June 2023 Editor: C.M. Petrone

Keywords: ignimbrite volcanism crustal evolution zircon geochronology zircon geochemistry

ABSTRACT

Large volume rhyolitic ignimbrite volcanism is a significant contributor to the evolving crust. The introduction of high-silica material into the upper crust, differentiation within the middle crust, and partial melting in the lower crust contributes to geochemical and isotopic evolution of the crust. Developing accurate models for the genetic evolution of these events is dependent upon geochronology to determine rates of magmatic processes as model constraints. We present new zircon high-precision CA-ID-TIMS U-Pb geochronology and MC-ICPMS Hf isotope geochemistry for four ignimbrites from the nested caldera complex near Socorro, New Mexico (USA), within the Mogollon-Datil volcanic field. In agreement with past ⁴⁰Ar-³⁹Ar data, interpretations of new U-Pb data indicate eruptions from the Socorro caldera cluster were pulsed. These pulses were intermittently spaced, and a volcanic hiatus following the Hells Mesa Tuff at 33.442 \pm 0.015 Ma was interrupted by four successive eruptions, beginning with the La Jencia Tuff at 29.158 \pm 0.025 Ma and finishing with the South Canyon Tuff at 28.066 \pm 0.021 Ma. Zircon age spectra became more protracted with each eruption, exhibiting age dispersions ranging from 0.347 Myr in the Hells Mesa Tuff to 4.502 Myr in the South Canyon Tuff. The increased dispersion is paralleled by an increase in the proportion of normally discordant grains, indicative of xenocryst incorporation. These protracted age spectra are not necessarily a function of thermal maturation in the middle to upper crust due to long-lived magma chambers. Rather, they are likely the result of increased melting of zirconbearing lower crust due to deep thermal maturation from repeated juvenile magma injections based on the incorporation of zircon material at the melt source. In contrast, the Hf isotope record is volumetrically dominated by autocrystic zircon domains and becomes more radiogenic through time, recording juvenile replenishment of the lower crust during progressive melting. Together, these data record the protracted evolution of the lower crust sampled by ignimbrites, lend insight into that evolution, and emphasize the need for detailed interpretation of high-precision datasets to advance volcanic models.

© 2023 The Author(s). Published by Elsevier B.V. This is an open access article under the CC BY license (http://creativecommons.org/licenses/by/4.0/).

1. Introduction

Geologic models are commonly restricted by the insufficient control on time: uncertain rates and durations are frequently our limitations in understanding of Earth. In magmatic systems this is particularly pertinent. Aspects such as magmatic lifespan, rate of magma accumulation, eruptive intervals, and timing of final solid-ification or eruption are all factors that have been used to define

E-mail address: sean.gaynor@princeton.edu (S.P. Gaynor).

and refine models for processes such as crustal differentiation, porphyry formation and supervolcano eruptions (e.g., Caricchi et al., 2014; Eddy et al., 2016; Chelle-Michou et al., 2017). The mineral zircon is the most commonly used material providing geochronological information to understand these processes, due its ability to incorporate appreciable U and its robust nature. Zircon records its crystallization in many silicic rocks because it tends to saturate in Si-rich magmas. Therefore, it may be exploited to derive the parameters of silicic magmatism, such as mechanisms of batholith formation, the transcrustal magmatic architecture, and age and duration of rhyolitic ignimbrite eruptions.

Through analytical advancements in both in-situ and high-precision methods, larger and increasingly precise U-Pb zircon

^{*} Corresponding author at: Department of Geosciences, Princeton University, Princeton, NJ, 08544, United States of America.

datasets continue to reveal more complicated and protracted age spectra that warrant careful interpretation. Zircon can crystallize through a broad temperature range, enabling protracted age spectra to be used to interpret a melt lifespan or T-t history of magmas (e.g., Samperton et al., 2017; Szymanowski et al., 2019; Curry et al., 2021). Alternatively, this observed scatter can be interpreted to indicate inheritance of older zircon components, either from previous batches of melts remobilized within a system (i.e., antecrysts) or from partial melting of ancient rock (i.e., xenocrysts; e.g., Miller et al., 2007: Samperton et al., 2015: Gavnor et al., 2022a), Interpretation of the zircon record within igneous rocks can be further obfuscated by analytical factors. Many in-situ techniques do not have the precision to analytically resolve the geological causes of dispersion and compositional variations in zircon, and as a result are unable to yield data with the uncertainties necessary to assess two-component mixing (e.g., Chelle-Michou et al., 2017; Gaynor et al., 2022a). Therefore, several common a priori assumptions of magmatic systems may be flawed, as zircon may not necessarily record a period of growth within an individual magma system (e.g., Wotzlaw et al., 2013; Karakas et al., 2019).

Beyond understanding the temporal evolution of the magma, zircon crystals can also lend insight about the generation of high silica melts. Melt evolution is commonly a complicated and varied process, and proxies such as trace element geochemistry can model the formation of silicic rocks through many mechanisms, including fractionation, partial melting, and entrainment processes (e.g., Bachmann and Bergantz, 2008; Glazner et al., 2008; Clemens et al., 2011). Zircon is robust, and chronicles crystallization throughout the history of a magmatic locus, recording the isotopic composition of its surrounding melt through Hf (e.g., Kinny and Maas, 2003; Schoene, 2014). Combined with U-Pb geochronology, zircon can be used to determine the composition of a given melt with a clear temporal understanding of a magma history.

Here we present a case study utilizing Hf and U-Pb zircon isotope geochemistry and geochronology from a suite of supervolcano eruptions to evaluate the lifespan of silicic magma systems as recorded by zircon. This dataset allows us to evaluate the differences in the duration of crystallization, degree of inheritance, and magma provenance through a long-lived magmatic center. For the geochronology, we used chemical abrasion, isotope dilution thermal ionization mass spectrometry (CA-ID-TIMS). This technique allows for a more precise evaluation of potential multicomponent mixing within individual crystals through assessment of $^{206}\text{Pb}/^{238}\text{U}-^{207}\text{Pb}/^{235}\text{U}$ concordance relative to in-situ techniques that inherently have larger analytical uncertainty. Therefore, it is more equipped to assess if crystal or sub-crystal dates obtained accurately reflect magmatic crystallization at a time of interest, or rather inheritance (e.g., Gaynor et al., 2022a). The CA-ID-TIMS technique is commonly applied to full zircon crystals, rather than discrete crystal volumes, and therefore produces a weighted average of the timing of crystallization, including possible trace inheritance. These analyses were followed by Hf isotope analyses by multi-collector inductively coupled plasma mass spectrometry (MC-ICPMS) on the same volume of zircon dated by CA-ID-TIMS, to test the magmatic provenance of individual crystals relative to their dates. We applied these techniques to a series of supervolcano eruptions from the Oligocene Socorro caldera complex, located in southern New Mexico, U.S.A. This natural laboratory is ideal for measuring the effects of ancient zircon material on younger eruptions because the basement for these rocks is over 1.5 Gyr older than the volcanic complex (e.g., Karlstrom et al., 2004). Our high-precision results highlight potential issues with commonly used interpretations of zircon spectra, while also allowing new insights into the generation and evolution of large volume, high-silica eruptions.

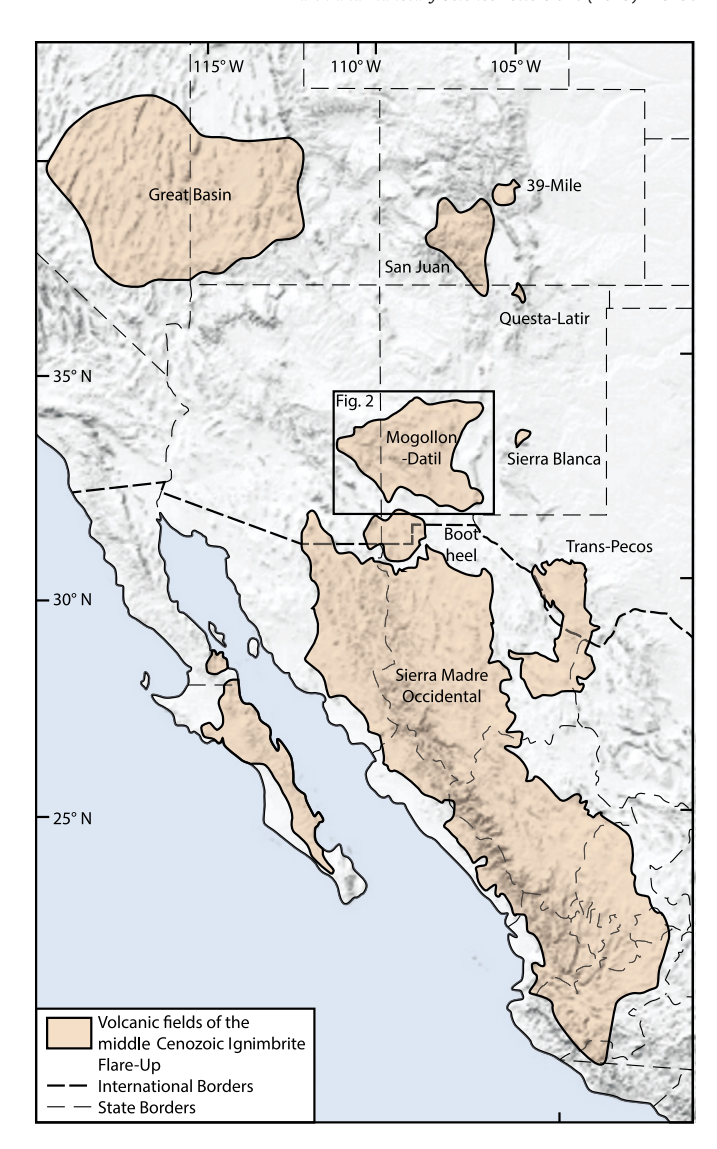


Fig. 1. Generalized map of the present-day extent of mid-Tertiary silicic volcanic fields of southwestern North America, highlighting the location of the 39-Mile, Boot Heel, Great Basin, Mogollon-Datil, Questa-Latir, San Juan, Sierra Blanca, Sierra Madre Occidental and Trans-Pecos volcanic fields. Modified from McIntosh et al. (1992), Cather et al. (2009) and McDowell and McIntosh (2012). Inset box indicates the location of Fig. 2.

2. Geological setting

The Socorro caldera cluster is located within the Mogollon-Datil volcanic field, which is part of the middle Eocene to middle Miocene ignimbrite flare-up of western North America. The ignimbrite flare-up is marked by a suite of discontinuous volcanic centers, stretching across approximately 3,500 km from central to southern North America, which was broadly active between 50-16 Ma (Fig. 1; e.g., Cather et al., 2009; McDowell and McIntosh, 2012). In many of these volcanic centers, early volcanism was predominately intermediate composition lava flows, which transitioned to large-volume, explosive felsic ignimbrite eruptions (Humphreys et al., 2003). In total, over 500,000 km³ of ignimbrites were erupted as part of at least 5,000,000 km³ of igneous rocks associated with this episodic magmatic flare-up, with the approximate peak flux of volcanism between 33-28 Ma (e.g., Johnson, 1991). Magmatism was focused between a suite of volcanic centers, including the Boot Heel, Great Basin, Mogollon-Datil, San Juan, and Sierra Madre Occidental volcanic fields (Fig. 1). Models for the magma genesis of these volcanic centers commonly involve the heating of

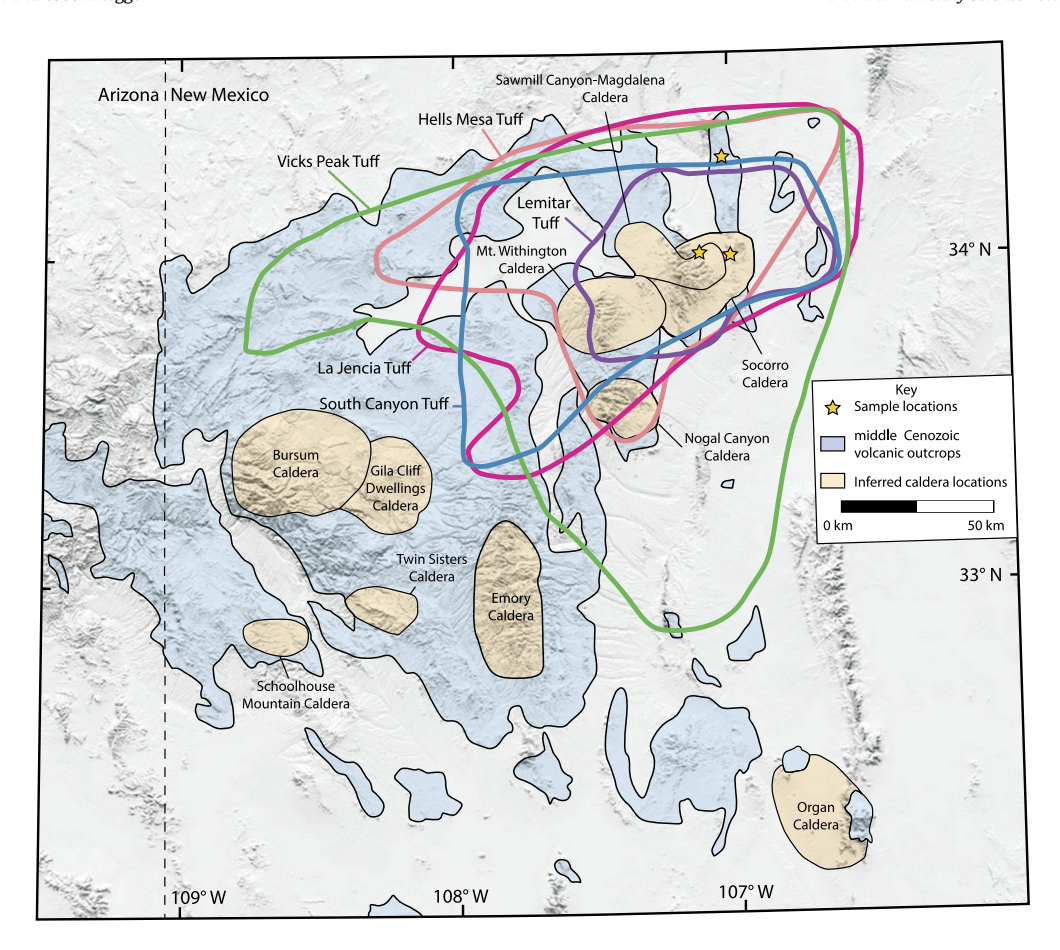


Fig. 2. Generalized geologic map of the Mogollon-Datil volcanic field in southern Arizona and New Mexico, showing the sampling sites for this study. Colored outlines reflect the mapped extent of individual large-volume ignimbrite eruptions from the caldera cluster adjacent to Socorro, which are based on paleomagnetic and ⁴⁰Ar/³⁹Ar data of distal ash samples from McIntosh et al. (1992). The colors used to indicate tuff extents correlate to the colors used to denote various ignimbrite samples in Figs. 3–6. Map modified from McIntosh et al. (1992) and does not include calderas associated with the Boot Heel volcanic field.

metasomatized North American lithosphere by upwelling asthenosphere during removal of the cooler Farallon slab (e.g., Davis and Hawkesworth, 1993; Humphreys et al., 2003; Farmer et al., 2008). These models postulate widespread melting, rapid introduction of voluminous mafic melts to the crust, and induced anatexis as a result of this upwelling.

Volcanic activity within the Mogollon-Datil volcanic field began with andesitic volcanism between approximately 40-36 Ma, and was followed by a suite of aerially extensive, voluminous rhyolite ignimbrites from approximately 36-24 Ma (Fig. 2; e.g., Cather et al., 1987; McIntosh et al., 1990, 1992). This latter phase of ignimbrite volcanism occurred episodically through four brief pulses separated by 1-3 Myr quiescences, with eruptions from 36.2-33.5 Ma, 32.1-31.4 Ma, 29.0-27.4 Ma and a final pulse at 24.3 Ma (e.g., McIntosh et al., 1990). The approximate eruptive volumes and rates vary between these pulses, with the third pulse responsible for the most volume and the highest eruptive rate of any ignimbrite pulses from the Mogollon-Datil volcanic field (e.g., McIntosh et al., 1992).

Along the northeastern margin of the Mogollon-Datil volcanic field lies a series of three nested calderas west of the town of Socorro: the Socorro, the Sawmill Canyon-Magdalena, and the Mt. Withington calderas, from east to west and oldest to youngest, respectively (Fig. 2; e.g., McIntosh et al., 1992; Chamberlin et al., 2004). Early volcanism locally predates caldera formation, beginning with the Datil Group volcanic rocks from approximately 39-33.7 Ma, which range from andesite to rhyolite in composition (McIntosh et al., 1992). The first phase of local ignimbrite volcanism began with the eruption of the 1,200 km³ Hells Mesa Tuff at 32.49 \pm 0.10/1.17 Ma, forming the Socorro caldera ($^{40} {\rm Ar}/^{39} {\rm Ar}$

sanidine geochronology recalculated from McIntosh et al., 1992; "x/z" uncertainties represent "analytical uncertainties only/including uncertainty of decay constants"). Smaller volume basalt and rhyolite flows ponded within the Socorro caldera during the period following the eruption of the Hells Mesa Tuff (Chamberlin et al., 2004). Following a period of resurgent dome emplacement along the caldera rim, the crystal poor 1,250 km³ La Jencia Tuff was erupted from the Sawmill Canyon caldera at 29.23 \pm 0.04/1.05 Ma (McIntosh et al., 1992; Chamberlin et al., 2004). The formation of the Sawmill Canyon-Magdalena caldera destroyed the western margin of the Socorro caldera (Chamberlin et al., 2004). The Nogal Canyon caldera formed south of the nested Socorro caldera complex through the eruption of the crystal poor, 1,050 km³ Vicks Peak Tuff at 28.94 \pm 0.04/1.04 Ma (Osburn and Chapin, 1983; McIntosh et al., 1992). The 450 km³ Lemitar Tuff subsequently erupted from the Hardy Ridge caldera, nested inside of the Sawmill Canyon-Magdalena caldera, at 28.37 \pm 0.08/1.02 (McIntosh et al., 1992; Chamberlin et al., 2004). The final phase of ignimbrite volcanism within the area is associated with the formation of the Mt. Withington caldera through the eruption of the 700 km³ South Canyon Tuff at 27.73 \pm 0.07/1.00 Ma (McIntosh et al., 1992; Chamberlin et al., 2004). The volumetric total of these ignimbrites is the largest estimated from a single caldera cluster within the Mogollon-Datil volcanic field (e.g., McIntosh et al., 1990, 1992).

3. Methods

Samples were collected from fresh outcrops of all five large volume, high silica ignimbrite eruptions associated with the Mt. Withington, Sawmill Canyon-Magdalena, Nogal Canyon and Socorro calderas (Fig. 2). All samples were crushed in a tungsten mill, sieved to less than 300 μm , and concentrated to heavy minerals using a Wilfley table, Frantz magnetic separation and heavy liquids. Due to the relative lack of zircon in the Vicks Peak Tuff, it was not processed or analyzed further. Backscattered electron (BSE) and cathodoluminescence (CL) images were acquired using a JEOL JSM7001F Thermal Field Emission Scanning Electron Microscope (SEM) (Schottky electron gun) at the University of Geneva. Mineral inclusions in zircon were identified using energy dispersive spectroscopy (EDS). These techniques were used to characterize the internal textures and the inclusions within representative crystals.

Zircon were prepared and analyzed for ID-TIMS U-Pb geochronology using the methods detailed in Appendix Text 1. Whole zircon crystals, rather than those sectioned and imaged using CL, were used in this study to maximize the radiogenic Pb to common Pb (Pb*/Pbc) values, which maximizes precision (e.g., Gaynor et al., 2022a). Zircons representing the range of crystal morphology were analyzed to fully characterize zircon in each sample. Reported ²⁰⁶Pb/²³⁸U dates were corrected for initial ²³⁰Th disequilibrium during zircon crystallization using a zircon/melt partition coefficient $f_{Th/U}$ of 0.246 (Rubatto and Hermann, 2007). Earthtime ET100 standard solution analyzed during the period of these analyses yielded a $^{206}\text{Pb}/^{238}\text{U}$ date of 100.1796 \pm 0.0066 Ma (MSWD = 2.1; n = 20), within uncertainty of the recently reported interlaboratory calibrated value of 100.173 \pm 0.003 Ma for this solution (Schaltegger et al., 2021). Unless otherwise noted, all U-Pb ages discussed in the text and figures are reported as Th-corrected ²⁰⁶Pb/²³⁸U ages.

Detailed methods for Hf isotope measurements can be found in Appendix Text 2. Data reduction to obtain the 176Hf/177Hf ratio included on-peak zero baseline correction, correction for mass bias induced by the mass spectrometer measurement, correction of isobaric interferences of ¹⁷⁶Lu and ¹⁷⁶Yb on ¹⁷⁶Hf, and an offset correction by adjusting the ¹⁷⁶Hf/¹⁷⁷Hf ratio of the sample for the observed difference between the measured (0.272172 \pm 0.000014, n = 67) and preferred value of the JMC475 Hf standard (i.e. 0.282160; Nowell et al., 1998). The average ¹⁷⁶Hf/¹⁷⁷Hf ratio of all measured Plešovice solutions during the period of sample analyses is 0.282479 \pm 0.000009 (n = 29), which translates to an $\varepsilon Hf_{(t)}$ value of -3.4 \pm 0.3 (2SD) at an age of 336.79 Ma (Widmann et al., 2019). This is identical within error to the proposed value in literature of $\varepsilon \mathrm{Hf_{(t)}}$ = -3.5 \pm 1.5 (Sláma et al., 2008). The average ¹⁷⁶Hf/¹⁷⁷Hf ratio of all measured Temora-2 solutions during the period of sample analyses is 0.282680 ± 0.000014 (n = 21), which translates to an $\varepsilon Hf_{(t)}$ value of 5.3 \pm 0.5 at an age of 417.353 Ma (Schaltegger et al., 2021), which is identical within error to the proposed value in literature of $\varepsilon Hf_{(t)}$ = 5.8 \pm 0.3 (Woodhead et al., 2004). The average ¹⁷⁶Hf/¹⁷⁷Hf ratio of all measured GJ-1 solutions during the period of sample analyses is 0.282009 \pm 0.000014 (n = 8), which translates to an $\varepsilon Hf_{(t)}$ value of -14.2 \pm 0.5 at an age of 600.28 Ma (Schaltegger et al., 2021), which is identical within error to the proposed value in literature of $\varepsilon Hf_{(t)}$ = -14.4 \pm 0.2 (Morel et al., 2008). All $\varepsilon Hf_{(t)}$ uncertainties discussed in the text and shown in figures are reported at the 2σ uncertainty level. For individual analyses with uncertainties below the variation of the secondary standards, we report those uncertainties as \pm 0.3 ε Hf_(t), which was the repeatability of Plešovice standards during the analytical period.

4. Results

Zircon crystals from all four bulk ignimbrites are typically euhedral and prismatic (Fig. A1). Representative grains imaged using cathodoluminescence exhibited textures including simple zonation,

oscillatory zoning and sector zoning, and many grains exhibited sharp contrast in CL response between zones (Fig. A2). Some imaged grains host mineral inclusions, such as apatite and feldspar.

4.1. ID-CA-TIMS U-Pb geochronology

Individual ²⁰⁶Pb/²³⁸U dates were Oligocene for all ignimbrites but span a considerable range and include a considerable number of normally discordant dates (Figs. 3 and 4; Table A1). A sample of the Hells Mesa Tuff (SLC21-2) yielded 16 dates ranging between 32.411 ± 0.080 and 32.758 ± 0.093 Ma ($\Delta t = 0.347$ Myr), with three normally discordant dates in the older portion of the spectra. Fifteen zircon dates from the La Jencia Tuff (SLC21-3) span between 29.153 \pm 0.029 and 30.09 \pm 0.25 Ma (Δt = 0.927 Myr), and all analyses are concordant within uncertainty except the oldest grain. Eighteen crystals from the Lemitar Tuff (BL21-1) gave dates ranging between 28.086 \pm 0.149 and 29.469 \pm 0.168 Ma (Δt = 1.383 Myr), with four normally discordant zircon and a plateau of 7 overlapping, concordant ages at the youngest portion of the age spectra. Finally, 21 zircon grains analyzed from the South Canyon Tuff (MMBT1) yielded $^{206}\text{Pb}/^{238}\text{U}$ dates between 28.024 \pm 0.079 and 32.526 \pm 0.028 Ma (Δt =4.502 Ma), with seven normally discordant zircon and three overlapping concordant analyses at the voungest portion of the age spectra.

4.2. MC-ICPMS zircon Hf isotope geochemistry

The Hf isotope composition of zircon crystals from the nested caldera cluster only yielded moderate dispersion, with no significant outliers (Fig. 5). Zircon from the Hells Mesa Tuff (SLC21-2) yielded compositions range from -5.7 \pm 0.9 to -7.4 \pm 0.7 ϵ Hf(t), with almost all analyses overlapping within uncertainty. The ϵ Hf(t) composition of fourteen zircon crystals from the La Jencia Tuff (SLC21-3) ranged from -5.8 \pm 0.7 to -7.1 \pm 0.5, with all analyses overlapping within uncertainty. Nineteen crystals from the Lemitar Tuff (BL21-1) yielded ϵ Hf(t) compositions ranging from -4.9 \pm 0.3 to -6.6 \pm 0.4, with more dispersion in ϵ Hf composition than observed in samples from the preceding two tuffs. Finally, zircon from the South Canyon Tuff (MMBT1) yielded ϵ Hf(t) compositions ranging from -5.2 \pm 0.3 to -7.0 \pm 0.8, with the most dispersion in ϵ Hf(t) compositions of all the samples studied here.

5. Discussion

Zircon from the Socorro caldera complex yields heterogeneous U-Pb dates and isotope compositions. Evaluation of these data indicates that the U-Pb geochronology does not necessarily record the evolution of magmas responsible for ignimbrite volcanism, but rather, reflects volumetric mixing of ancient zircon material with autocrystic zircon. The Hf isotope record is decoupled from the geochronology, reflecting the composition of magmas during the crystallization of autocrystic zircon due to volumetric mixing. Overall, these data highlight the need for detailed, careful evaluation of protracted age spectra when developing models for igneous systems, while demonstrating the subtle, yet important, magma genesis information hidden within the complicated zircon crystal record.

5.1. Interpretation of U-Pb zircon ages from the Socorro caldera complex

Age spectra from samples of the Socorro caldera complex present varying degrees of complexity, all samples yielded age variance beyond a single statistical population. Therefore, estimating eruption ages of individual ignimbrites from such scattered dates requires careful interpretation. Protracted age spectra within

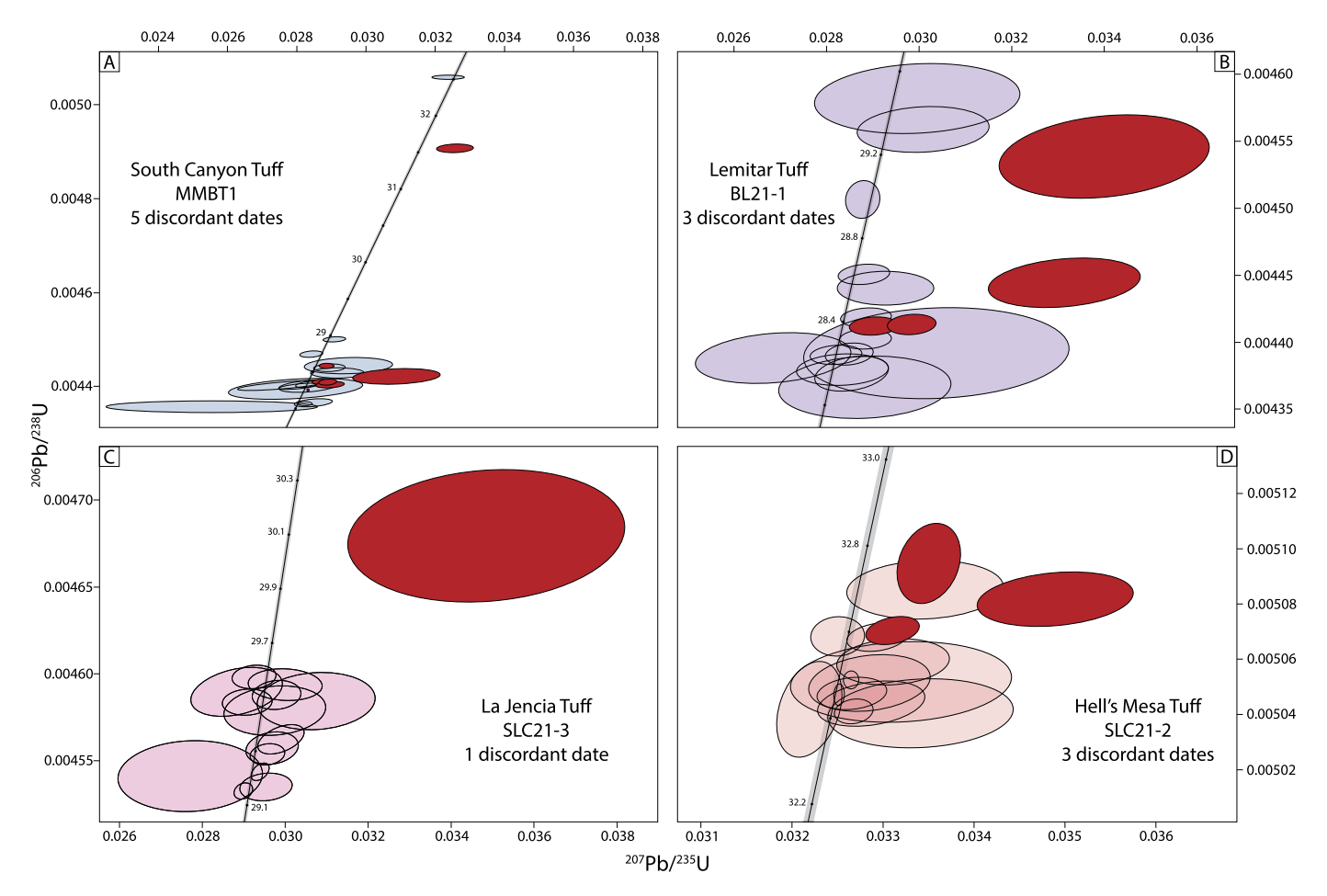


Fig. 3. Zircon U-Pb CA-ID-TIMS results for samples of ignimbrite eruptions from the Socorro caldera cluster displayed on a Wetherill concordia. Normally discordant analyses are displayed in red, to highlight the relative abundance of these analyses as well as their location in concordia space. Each concordia plot is shown at a different scale, in order to encompass all of the U-Pb data for each sample. Note that the most precise analysis within the dataset, the fourth youngest ²⁰⁶Pb/²³⁸U date in the sample of the South Canyon Tuff (NMBT1) is normally discordant. See text for further discussion.

individual igneous samples can be caused by several factors, including: (1) unmitigated Pb-loss due to non-ideal conditions of chemical abrasion, such as in cases of very U-rich and metamict zircon, leading to inaccurately young crystallization ages, (2) prolonged zircon growth within a single magma reservoir (autocrysts). (3) inheritance of zircon and/or domains of zircon from previous magmas within a long-lived magmatic locus (antecrysts), or (4) inheritance of ancient zircon from either wall rock or the anatectic source (xenocrysts; e.g., Miller et al., 2007). The 12 hour, 210 °C chemical abrasion pretreatment used in this study has been shown to be effective in mitigating Pb-loss (e.g., Widmann et al., 2019). None of the samples' age spectra yielded anomalously young ages, and the youngest ages in the zircon spectra overlap within uncertainty with the existing Ar-Ar geochronology (Fig. 4). We thus conclude that Pb-loss is not a component causing apparent age scatter.

The remaining three mechanisms, (1) prolonged autocrystic zircon growth, and inclusion of (2) antecrystic, or (3) xenocrystic zircon material, can all result in protracted age spectra with individual zircon dates within a volcanic rock that significantly predate the period of eruption (e.g., Wotzlaw et al., 2013; Curry et al., 2021; Gaynor et al., 2022a). Xenocrystic zircon mixtures (i.e., mixing of two U-Pb reservoirs with distinctly different isotopic compositions), commonly yield normally discordant analyses when analyzed with sufficient precision (e.g., Wotzlaw et al., 2015; Gaynor et al., 2022a). A total of fifteen normally discordant dates are distributed across the four samples presented here, and all yielded 206Pb/238U dates older than the youngest grain in their respec-

tive sample. Therefore, we interpret each sample to host a variable abundance of xenocrystic inheritance, which can increase the total duration of dates in a sample and vield dates that do not reflect the magmatic history of their host eruptive rocks. It is also possible that more grains analyzed in this study include xenocrystic inheritance, but our inability to identify their potential inheritance is due to analytical uncertainty. The ability to resolve discordance is commonly a function of precision, which is directly related to the ratio of radiogenic Pb to common Pb (Pb*/Pbc) in high-precision CA-ID-TIMS analyses (Gaynor et al., 2022a). Many of the zircon analyses from samples in this study exhibit rather low Pb*/Pbc values (<10) due to their lower U abundances and insufficient time for radiogenic ingrowth. Therefore, individual dates may be apparently concordant due to higher ²⁰⁷Pb/²³⁵U uncertainty, but still yield ²⁰⁶Pb/²³⁸U dates older than magmatic crystallization of interest due to xenocrystic inheritance. For example, zircon MMBT1 Z6 has the highest Pb^*/Pb_c within this dataset $(Pb^*/Pb_c = 91.99)$ and is normally discordant (Fig. 3), however if it had the average composition of this dataset (Pb*/Pbc = 10.46), then it would be concordant within uncertainty.

The remaining two possible drivers of the observed protracted age spectra, antecrystic inheritance and protracted autocrystic growth, are often associated with concordant zircon dates older than the final phase of zircon crystallization. It is likely that all four samples in this study are also affected by these two mechanisms, as they all have concordant zircon dates far beyond the threshold of a single statistical population. However, given the available level of precision, it is not possible to analytically determine if

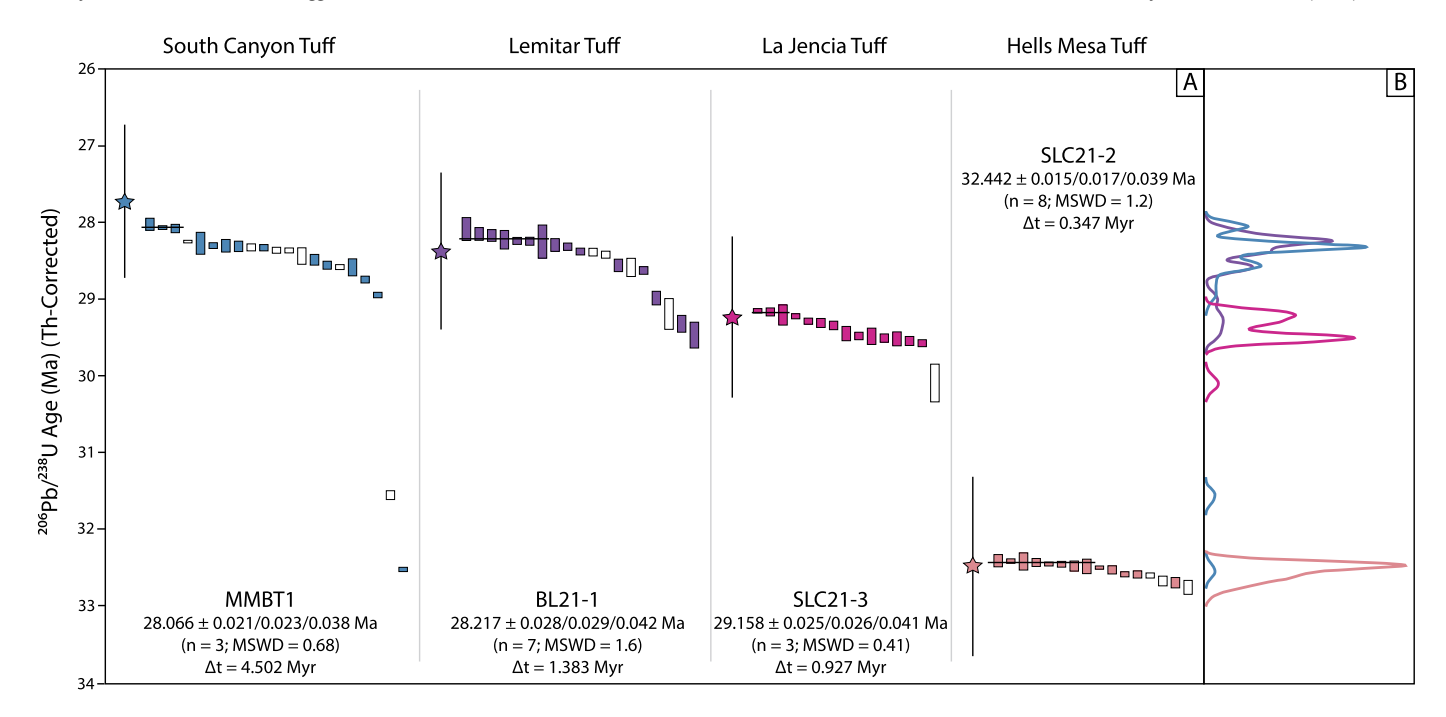


Fig. 4. 206 Pb/ 238 U dates for individual zircons from ignimbrite samples of the Socorro caldera cluster, along with interpreted weighted mean estimates for eruptions (**A**), and kernel density estimates (KDEs) of the age spectra from each sample (**B**). Vertical bar heights are 2σ analytical uncertainties for individual analyses. Unfilled boxes represent normally discordant zircon analyses, all other analyses are concordant. Weighted mean interpreted ages for each ignimbrite eruption are presented with X/Y/Z notation, where X = analytical error only/Y = analytical error with uncertainty of spike calibration added/Z = analytical error with uncertainty of spike calibration added and uncertainty of spike calibration added and uncertainty of kuiper et al. (2008). Uncertainties shown for the 40 Ar/ 39 Ar analyses incorporate decay constant uncertainties, zircon data only show the analytical uncertainties associated with U-Pb dates. The Δ t values presented with each sample reflect the difference between their oldest and youngest 206 Pb/ 238 U dates. See text for discussion.

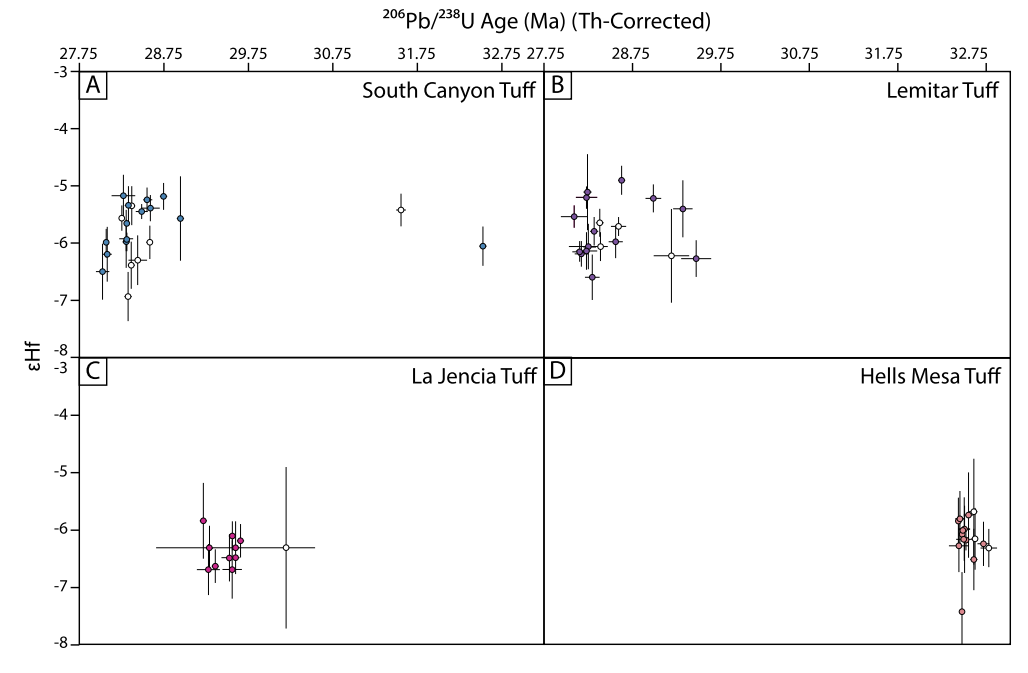


Fig. 5. Comparison of the Hf isotope geochemistry and 206 Pb/ 238 U dates of individual zircon crystals from ignimbrite eruptions of the Socorro caldera cluster, including (**A**) the South Canyon, (**B**) Lemitar, (**C**) La Jencia and (**D**) Hells Mesa tuffs, in order of youngest to oldest. Both the horizontal and vertical bar heights are 2σ analytical uncertainties for individual analyses. Unfilled circles indicate zircon which yielded normally discordant analyses. In some cases, uncertainty of the 206 Pb/ 238 U dates on individual analyses is smaller than the symbols used in the figure. There is not a correlation between the dates and Hf isotope geochemistry in any of the ignimbrite zircon analyzed.

some of the older concordant analyses are either: (1) the result of mixing with variable volumes of recently crystallized zircon components associated with a shared magmatic history (antecrysts or autocrysts), or (2) the result of mixing with a volumetrically insignificant amount ancient zircon (xenocrysts). Therefore, rather than incorporate these protracted dates into interpretation of a ge-

ologically significant age, we interpret that the youngest cluster of overlapping, concordant analyses reflect final zircon crystallization within individual samples, thereby approximating the timing of ignimbrite eruption (Fig. 4). Using this interpretation strategy, we interpret that the Hells Mesa Tuff erupted at $32.442 \pm 0.015/0.017/0.039$ Ma (SLC21-2; n = 8; MSWD = 1.2), La Jencia Tuff

erupted at 29.158 \pm 0.025/0.026/0.041 Ma (SLC21-3; n = 3; MSWD = 0.41), Lemitar Tuff erupted at 28.217 \pm 0.028/0.029/0.042 Ma (BL21-1; n = 7; MSWD = 1.6) and South Canyon Tuff erupted at 28.066 \pm 0.021/0.023/0.038 Ma (MMBT1; n = 3; MSWD = 0.68). These values only record the final crystallization of zircon within each of the samples of volcanic rock studied here, and therefore may be older than the exact timing of eruption. However, due to their overlap with recalculated $^{40}\text{Ar}/^{39}\text{Ar}$ geochronology, we are confident in this interpretation (Fig. 4).

As an alternative way to interpret a geologic age from complicated zircon dates, recent work has suggested that integrating the full range of zircon dates from given samples into statistical models, including autocrysts and antecrysts, can resolve the thermal history of a system and yields the most probable solidification or eruptive age integrated from the full zircon crystallization history (e.g., Samperton et al., 2017; Keller et al., 2018). Many of these models are predicated on all individual dates accurately recording the magmatic processes that lead to the solidification of that igneous rock. The presence of normally discordant dates from tuffs of the Socorro caldera cluster do not support this assumption, and therefore this dataset may serve as an example of how the inappropriate application of these models can lead to spurious and inaccurate interpretations of ages. Many of the older dates within age spectra in this study are interpreted to contain a xenocrystic component, which indicates that not all ²⁰⁶Pb/²³⁸U dates necessarily reflect magmatic growth. The incorporation of dates from xenocryst-bearing zircon artificially extends the growth history and has the ability to produce younger modeled eruption or solidification ages. For example, applying the Bayesian modeling of Keller et al. (2018) to the South Canyon Tuff yields an eruption age of 27.851 \pm 0.112 Ma, approximately 200 kyr younger than the weighted mean plateau (Table A3). While both age interpretations agree with the previously published 40 Ar/39 Ar geochronology due to its large uncertainty, the interpretation generated from the Bayesian model would also suggest that there is not a zircon record within our CA-ID-TIMS dataset of the final 100-300 kyr of magmatic evolution of the South Canyon Tuff prior to eruption. This is unlikely, as thermal modeling and high-precision zircon studies suggest that the pre-eruptive residency of individual eruptive magma bodies is on the scale of 10 s to 100 s of kyr, after which most silicic magmas reach rheological lock up and are no longer capable of eruption (e.g., Schöpa and Annen, 2013; Barboni and Schoene, 2014; Rioux et al., 2016; Schaen et al., 2021; Pamukçu et al., 2022). In some cases, when full textural characterization of zircon is combined with high-precision dating and additional geochemical data, it may be possible to validate the assumptions necessary to use this sort of modeling approach to interpret a geologic age of an igneous event. Given the data from the Socorro caldera cluster, we urge caution with future work applying this technique or similar techniques to complicated age spectra, as many datasets may not have the precision or additional information necessary to validate the fundamental assumptions needed to justify this modeling approach.

5.2. Implications for magma genesis from protracted age spectra from Socorro ignimbrites

There is significant temporal overlap within individual ²⁰⁶Pb/²³⁸U age spectra of the different ignimbrite samples in this study, particularly between the South Canyon and the Lemitar tuffs (Fig. 4); this kind of evidence has been used in many studies to indicate that these igneous rocks may have shared a similar crystal cargo of zircon, and potentially a shared genetic history (e.g., Wotzlaw et al., 2013; Gaynor et al., 2019; Szymanowski et al., 2019; Curry et al., 2021; Pamukçu et al., 2022). More specifically, these models bear on the space- and time-resolved presence of

magmatic liquid, the total lifespan of transcrustal or upper crustal magma systems, and the timeframe required for the magmatic assembly of a supervolcano. Therefore, based on the nearly continuous zircon dates from the La Jencia, Lemitar, and South Canyon tuffs (Figs. 3 and 4), application of this interpretive model would suggest that the Socorro caldera cluster eruptions were fed from a common, long-lived magmatic system that was active on a scale of 100s to 1,000s of kyr with significant melt fractions for almost 2 Myr.

However, the interpretation offered above ignores a fundamental aspect of these data: all analyzed zircon populations are complicated by the presence of xenocrystic zircon domains, identified through complicated CL imagery and normal discordance (Figs. 3 & A2). While the presence of two separate decay chains is a unique strength that allows for detection of multicomponent mixing in U-Pb geochronology, the ability to do so is contingent on the precision achieved during analysis (Gaynor et al., 2022a). The overlap of the ²⁰⁶Pb/²³⁸U dates of many grains analyzed in this study may be due to variable volumetric mixing of autocrystic and xenocrystic domains within the crystals, rather than actual coeval crystallization of either autocrystic or antecrystic zircons sampled by different eruptive cycles. The mixing of autocrystic and xenocrystic domains scenario is supported by normally discordant analyses of ²⁰⁶Pb/²³⁸U dates that overlap with both concordant and further normally discordant dates among the La Jencia, Lemitar, and South Canyon tuffs (Fig. 3). There are also older concordant grains within these age spectra, which may either include antecrystic inheritance from earlier stages within the magmatic locus or inheritance of xenocrystic zircon with ²⁰⁷Pb/²⁰⁶Pb younger ages such that discordance is not analytically resolved. Based on the obvious presence of xenocrystic inheritance, the overlapping zircon age spectra from different ignimbrite eruptions likely do not indicate a shared, longlived parental magma system or preserve a thermal record of the magmatic locus, and it may be wrong to interpret that the concordant analyses all reflect accurate magmatic dates. Instead, we suggest it only demonstrates that all ignimbrite magmas of interest host minor amounts of xenocrystic inheritance, and that overlap between the age spectra of different eruptions is just a function of that inheritance.

While the abundance of normally discordant zircon does not necessarily inform us about the magmatic evolution of this volcanic center, it does bear on the evolution of the ignimbrite flare-up. There is an overall increase in the abundance of normally discordant zircon throughout the eruptive sequence of the caldera cluster, paralleled by an increase in the dispersion of the age spectra (Δt ; Fig. 4). The oldest $^{206}\text{Pb}/^{238}\text{U}$ date in each sample is not necessarily normally discordant. However, samples with more protracted spectra also tend to contain more normally discordant dates, suggesting that progressively higher Δt values result from the increasing presence of xenocrystic content. The two mechanisms to incorporate xenocrystic zircon into a melt are either through assimilation of crustal wall-rock via assimilation (e.g., Gaynor et al., 2022b), or entrainment during lower crustal anatexis (e.g., Clemens et al., 2011). Assimilation thermodynamically induces crystallization of the host magma (Glazner, 2007), such that a significant proportion of zircon material liberated from wallrock will be unlikely to mix into the pre-eruptive magma system and become incorporated into ascending, pre-eruptive antecrystic or autocrystic zircon growth. Entrainment of zircon material commonly occurs during partial melting (e.g., Clemens et al., 2011), suggesting that anatexis of zircon bearing lower crust is the primary way to introduce xenocrystic material to magmas. Therefore, we interpret the increasing xenocrystic zircon content with time in the Socorro caldera cluster ignimbrites to record increasing degrees of anatexis of zircon-bearing lower crust during the magma genesis of later magmas.

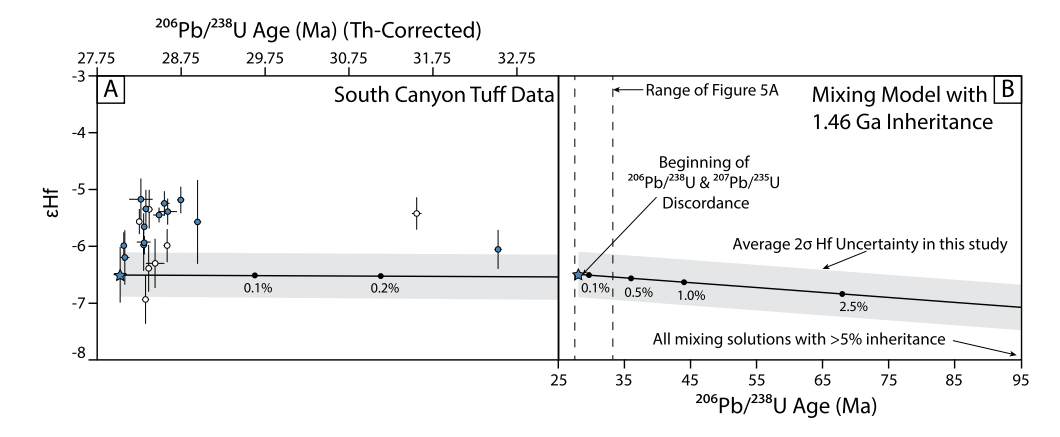


Fig. 6. Comparison of the Hf isotope geochemistry and 206 Pb/ 238 U dates of individual zircon crystals from the South Canyon tuff (A) and an isotope mixing model between the youngest zircon in that dataset (Z4) with 1.46 Ga xenocrystic inheritance (B). (A) For the data from the South Canyon Tuff, both the horizontal and vertical bar heights are 2σ analytical uncertainties for individual analyses. Unfilled circles indicate zircon which yielded normally discordant analyses. In some cases, uncertainty of the 206 Pb/ 238 U dates on individual analyses is smaller than the symbols used in the figure. (B) Volumetric mixing model of the U-Pb and Hf isotope systems, highlighting the relative inability to resolve subtle xenocrystic inheritance through Hf isotopes relative to the ability to resolve discordance between 206 Pb/ 238 U and 207 Pb/ 235 U. The line reflects the continuous solution of mixing between the two tested end-members (e.g., 0.1% xenocrystic inheritance, 99.9% autocryst per volume). The dashed lines show the entire range of plot in Fig. 6A. However, the Hf isotopic composition of the mixed product does not change beyond uncertainty within the range of either plot. Note: the analytical limitations shown in this figure, both for 2σ Hf and the ability to resolve discordance between 206 Pb/ 238 U and 207 Pb/ 235 U, only apply to CA-ID-TIMS and solution MC-ICPMS, less precise techniques are unable to resolve these geologic complications at the levels shown here. See text for discussion.

The data presented here record lower crustal processes during the evolution of the ignimbrite-producing center that formed the Socorro caldera cluster, rather than purely reflecting its middle to upper crustal magmatic history. In this proposed model, changes in zircon geochronology through the eruptive sequence are a function of magma genesis rather than magma evolution; driven by changes in melting alongside changes in crystallization. Therefore, xenocrystic domains stored in some zircon crystals retain important information about the melt generation. Moreover, wholesale application of these or similar U-Pb datasets to thermal-magmatic history modeling of eruptive rocks is inappropriate because the magmatic historical record is adulterated by older material.

One of the reasons the xenocrystic domains in this study are resolvable through normal discordance is because of the significant age difference between the volcanic rocks and their potential anatectic sources. The Socorro caldera cluster is located within a Proterozoic terrane composed largely of 1.4 and 1.6 Ga basement (Karlstrom et al., 2004). Therefore, mixing between basement age zircons and the Oligocene magmatism decouples ²⁰⁶Pb/²³⁸U and ²⁰⁷Pb/²³⁵U systematics such that two-component mixing is visible in concordia space. In young volcanic arcs, the potential offset between the two isotopic decay schemes may be analytically unresolvable due to the small temporal difference between the two age components. Furthermore, less precise analytical techniques, such as laser ablation inductively coupled plasma mass spectrometry (LA-ICPMS) or secondary ion mass spectrometry (SIMS), may not yield the precision to sufficiently assess concordance. Therefore, we urge extreme caution when using analytically protracted zircon age spectra for modeling magma evolution, as many of the data points used may not be faithful to the melt of interest.

5.3. Zircon Hf isotope record of ignimbrite generation

A further way to assess genetic relations between the zircon crystal loads of successive eruptions is comparison of the U-Pb and Hf isotope systematics from Socorro caldera zircon. In particular, the Hf isotopic compositions of dated zircon have the ability to potentially identify xenocrystic components of crustal, non-radiogenic origin or trace the magma composition from which zircon crystallized. In theory, this provides a tool to determine which portions of a protracted age spectra specifically relate to the magmatic history, allowing for the identification of the magmatic dates and compo-

sitions to model melt evolution. If ancient, inherited zircon cores are the cause for older U-Pb dates, then the Hf isotope composition of those grains should be less radiogenic (e.g., Hawkesworth and Kemp, 2006). However, there is no correlation between zircon dates and Hf isotope compositions, regardless of U-Pb concordance. Rather, the data show a range of Hf compositions independent of date in all four samples (Fig. 5).

Recent work has demonstrated that high-precision CA-ID-TIMS U-Pb data can detect two-component mixing with excellent analytical precision (Gaynor et al., 2022a). Therefore, we can test the sensitivity of Hf isotope compositions relative to U-Pb dates through a mixing model involving the youngest concordant zircon analyzed from the South Canyon tuff (Z4; $^{206}\text{Pb}/^{238}\text{U} = 28.024 \pm 0.079 \text{ Ma}$, $\varepsilon Hf_{(t)}$ = 6.5 \pm 0.5) and a hypothetical inherited 1.46 Ga zircon with $\varepsilon Hf_{(t)}$ = -20, typical of basement in and around the Socorro caldera cluster (Karlstrom et al., 2004; Goodge and Vervoort, 2006) as endmembers. This simple binary mixing model shows that mixing less than 0.1% of the Proterozoic zircon composition significantly shifts the 206Pb/238U age towards older values, well beyond the precision resolved by CA-ID-TIMS and yields normal discordance within the U-Pb system (Fig. 6). Conversely, the Hf isotope composition of these hypothetically mixed grains still overlaps within uncertainty with the Oligocene end-member, given the average 0.4ε 2σ uncertainties found in this study (Fig. 6). In this model, a Hf isotope composition that would resolve the two-component mixing (i.e., no overlap with the Oligocene Hf composition within uncertainty), would correspond to a normally discordant ²⁰⁶Pb/²³⁸U date of 120.36 Ma, which is much older than any grain analyzed in this study. Furthermore, given the age difference between the Proterozoic basement and the Cenozoic volcanic rocks, xenocrystic inheritance was likely minor and contributed significantly less than 1% volume to individual crystals in this model. Otherwise, zircon ages would be much older (Fig. 6). While the subtle level of xenocrystic inheritance observed in our data is resolvable by high-precision U-Pb CA-ID-TIMS analyses and revealed by normal discordance in these data (Fig. 3), it is not resolvable in the Hf data due to the analytical limitations (Fig. 6).

Based on this mixing relationship, the measured Hf isotopic compositions in this study are unresolvable from their dominant volumetric mixing component, and therefore reflect the composition of the autocrystic/antecrystic domains or grains within measurement uncertainty. This indicates that the heterogeneity of Hf

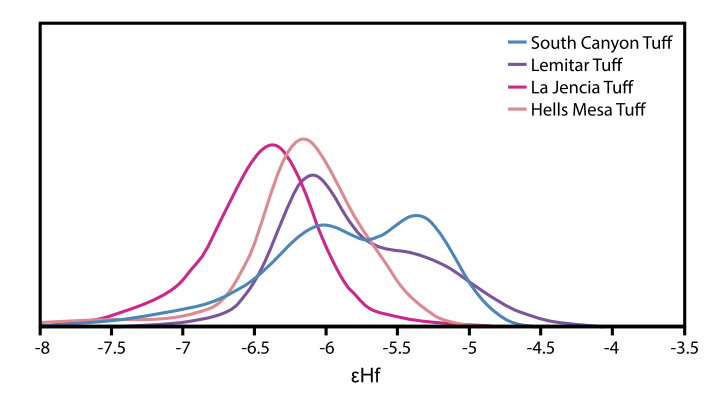


Fig. 7. Kernel density estimate (KDE) diagram of Hf isotope geochemistry of individual zircon crystals from the four ignimbrite eruptions analyzed from the Socorro caldera cluster: the South Canyon, Lemitar, La Jencia and Hells Mesa tuffs, from youngest to oldest. Note the younging trend of the data becoming more dispersed and juvenile through successive eruptions. We interpret this to record the magma sources becoming more heterogeneous and incorporating more juvenile input through time. See text for discussion.

isotope compositions between zircon grains of slightly different ²⁰⁶Pb/²³⁸U dates records variability in Oligocene magmatic processes, and likely holds important information about the magmatic composition(s) of ignimbrite magmas during zircon crystallization (Figs. 5 and 7). Zircon Hf isotope compositions of the first two eruptions, the Hells Mesa and La Jencia tuffs, are characterized by little dispersion, with mean values at approximately -6.2 and -6.5 ε Hf, respectively. Next, the younger Lemitar Tuff has a main population of zircon with compositions around -6.2 ε Hf, with a lesser population at approximately -5.3 ε Hf. Finally, the youngest volcanic unit in this study, the South Canyon Tuff contains zircons that are essentially bimodal, with populations at -6 and -5.25 ε Hf. Through the approximately 4.4 Myr eruptive sequence, zircons exhibit increasing heterogeneous Hf isotope compositions within individual eruptions, and there is an overall shift towards more positive values. Therefore, the magmatic inputs for these successive ignimbrite eruptions became more heterogeneous through time and incorporated increasingly juvenile sources. This is consistent with previous work that documented a trend towards increasingly juvenile magma sources through the evolution of the Rio Grande rift system (Lawton and McMillan, 1999; McMillan et al., 2000).

5.4. Sampling Myr scale lower crustal evolution through ignimbrite zircon

Zircon from the Socorro caldera cluster reflect the broader evolution of ignimbrite magma genesis over the course of approximately 4.3 Myr, and a period of significant change in magma genesis over approximately 1.1 Myr. Combining U-Pb and Hf isotope systems in these crystals yield three major observations of the evolving magma genesis for the Socorro caldera cluster: (1) increased juvenile magmatic input through time identified through Hf isotopes (2) increasing heterogeneity in Hf isotope compositions, and (3) increased incorporation of ancient crustal material through entrainment of zircon material.

Models for the Oligocene-Miocene magmatic flare-up in southwestern North America, which the Socorro caldera cluster is a part of, propose the introduction of large volumes of lithospheric mantle melt to the lower crust, and both domains contributed to subsequent ignimbrite magmatism (e.g., Farmer et al., 2008). Thermal modeling of lower crustal melting indicates that the ability to generate protracted magmatism, such as the 4.3 Myr of ignimbrite volcanism of the Socorro caldera cluster, requires prolonged melt injections (e.g., Annen et al., 2006). Therefore, to generate the observed magmatism, the lower crust would have been repeatedly

intruded by juvenile melts, hybridizing the lower crust through time, and driving a compositional change. As the region of melting increasingly incorporated juvenile material, subsequent melting events had an increased ability to incorporate this newly injected material, either through remelting or directly contributing to ascending melts. This signal is reflected in the overall shift towards more juvenile Hf isotope compositions through successive ignimbrites (Fig. 7).

The later phases of melt generation also sampled a more heterogeneous suite of source rocks, due to this process of progressive mafic injection (Fig. 7). Continued structurally deep addition of juvenile melts would progressively provide heat and volatiles, allowing for crustal melting of the regions surrounding mafic injections, assimilating more evolved compositions into the region of magma genesis (e.g., Petford and Gallagher, 2001; Annen and Sparks, 2002). Given the relatively non-radiogenic Hf composition of crustal reservoirs, it is unlikely that these domains were the dominant contributions to the zone of magma genesis once readily fusible through conditions induced by juvenile recharge in the deep crust. Rather, isolated regions of assimilation contributed lesser percentages to the overall plumbing network of magma genesis but were unable to be thoroughly mixed during ascent and crystallization prior to eruption. Similar models have been applied to interpret complicated zircon geochemistry during extensive granite formation in the upper crust (Farina et al., 2018). Zircon from the Socorro caldera cluster ignimbrites records a suite of diverse melt signatures during large scale melting of heterogeneous sources, which eventually coalesced into a magma body that produced ignimbrite eruptions, sampling more diverse source rocks during progressive melting due to continued addition of heat and volatiles.

This more heterogeneous phase of melting is also revealed through increasing xenocrystic inheritance in zircon through successive eruptions, indicative of incorporation of more zircon bearing rocks during magma genesis (Fig. 3). Modeling suggests that new zircon crystals may not immediately begin crystallizing upon saturation, and the ability to nucleate new crystals is inhibited by proximity to other zircon crystals (Sorokin et al., 2022). Therefore, any domains of xenocrystic zircon introduced to the magma system via anatexis likely serve as nucleation points for subsequent crystal growth, the earliest sites of potential zircon growth following magmatic saturation of the phase. The size and abundance of these components available for subsequent zircon crystallization is a function of source rock and magma composition as well as duration of time spent in zircon dissolving conditions, and therefore the increasing abundance of xenocrystic components through the evolution of the magmatic center serves as a distinct signature of changing magma provenance through time. Overall, these zircon isotope signals reflect the fundamental restructuring of the lower crust through the generation of caldera forming magmatism, revealing short-term geochemical evolution of the crust.

6. Conclusions

High-precision CA-ID-TIMS U-Pb geochronology and MC-ICPMS Hf isotope geochemistry of zircon from four ignimbrites of the nested caldera complex near Socorro, New Mexico yielded complicated isotope geochronology and geochemistry, with analytically resolvable scatter. The intrasample ²⁰⁶Pb/²³⁸U age variations are at least partially due to the incorporation of ancient zircon material during crystallization. However, resolving this inheritance through normal discordance is only possible due to the significant age difference between Proterozoic basement material and Oligocene volcanic rocks, and the high precision of this dataset. The scatter in initial Hf isotope compositions is unlikely to have been caused by this contamination based on simple binary mix-

ing. Instead, it reflects the isotopic heterogeneity of the melts that crystallized zircon prior to ignimbrite eruption, and Hf isotopes are unlikely to reveal subtle xenocrystic inheritance. Together, these data highlight the issues with models that infer extended lifespans for igneous plumbing systems based on protracted age spectra, as they may not accurately record the magmatic history. This is because the protracted nature of these age spectra may be due to cryptic inheritance of volumetrically minor material, vielding inaccurate estimates and rates of magmatic histories. Models that do not consider xenocrystic inheritance potentially miss the critical geologic signal within these protracted age spectra of magma genesis captured through inclusion of incomplete dissolution of anatectic products. In the Socorro caldera cluster, the increasing abundance of inherited zircon through the eruptive sequence indicates a shift in magma genesis through time, incorporating more partial melting of zircon bearing rock. This is paralleled by a shift in initial Hf isotope compositions. This shift indicates that the overall composition of the melt zone for the eruptive sequence became more juvenile through time. This likely drove volcanism as progressive injections of mafic material into the lower crust melted increasingly heterogeneous material, recording deeper processes than upper crustal crystallization. These data highlight that the zircon cargo of igneous rocks may not just record crystallization of magma from the onset of zircon saturation, but also contain a detailed history of igneous rock, which stretches from magma genesis to final solidification.

CRediT authorship contribution statement

Sean P. Gaynor: Conceptualization, Formal analysis, Investigation, Writing - original draft, Writing - review & editing. Tyson M. Smith: Resources, Writing - review & editing. Urs Schaltegger: Funding acquisition, Writing - review & editing.

Declaration of competing interest

The authors declare that they have no known competing financial interests or personal relationships that could have appeared to influence the work reported in this paper.

Data availability

Data will be made available on request.

Acknowledgements

This research was supported by the Swiss National Science Foundation project No. 200020 182007 to U.S. Hafnium isotope measurements benefited from support from Massimo Chiaradia, zircon mounts were supported by Jean-Marie Boccard, SEM imagery was supported by Agathe Martignier, and mineral separation work was supported by Mélissa Ruiz. Field work was supported by Magdalena A. E. Curry through North Carolina State University and University of Houston. Thanks to reviewers Philip Leat and Michael Eddy, as well as an internal USGS review by Josh Rosera, for constructive and very thorough reviews of this manuscript. Thanks to Editor Chiara Maria Petrone for the handling of this manuscript. Any use of trade, firm, or product names is for descriptive purposes only and does not imply endorsement by the U.S. Government.

Appendix A. Supplementary material

Supplementary material related to this article can be found online at https://doi.org/10.1016/j.epsl.2023.118236.

References

- Annen, C., Sparks, R.S.I., 2002. Effects of repetitive emplacement of basaltic intrusions on thermal evolution and melt generation in the crust. Earth Planet. Sci.
- Annen, C., Blundy, J.D., Sparks, R.S.J., 2006. The genesis of intermediate and silicic magmas in deep crustal hot zones. J. Petrol. 47, 505-539.
- Bachmann, O., Bergantz, G.W., 2008. Rhyolites and their source mushes across tectonic settings. J. Petrol. 49, 2277-2285.
- Barboni, M., Schoene, B., 2014. Short eruption window revealed by absolute crystal growth rates in a granitic magma. Nat. Geosci. 7, 524-528.
- Caricchi, L., Simpson, G., Schaltegger, U., 2014. Zircons reveal magma fluxes in the Earth's crust. Nature 511, 457-461.
- Cather, S.M., McIntosh, W.C., Chapin, C.E., 1987. Stratigraphy, age, and rates of deposition of the Datil Group (Upper Eocene-Lower Oligocene), west-central New Mexico. New Mex. Geol. 9, 50-54.
- Cather, S.M., Dunbar, N.W., McDowell, F.W., McIntosh, W.C., Scholle, P.A., 2009. Climate forcing by iron fertilization from repeated ignimbrite eruptions: the icehouse-silicic large igneous province (SLIP) hypothesis. Geosphere 5, 315–324. Chamberlin, R.M., McIntosh, W.C., Eggleston, T.L., 2004. ⁴⁰Ar/³⁹Ar geochronology and
- eruptive history of the eastern sector of the Oligocene Socorro caldera, central Rio Grande rift, New Mexico. New Mex. Bur. Geol. Miner. Resour. Bull. 160, 251-279
- Chelle-Michou, C., Rottier, B., Caricchi, L., Simpson, G., 2017. Tempo of magma degassing and the genesis of porphyry copper deposits. Sci. Rep. 7, 1-12.
- Clemens, J.D., Stevens, G., Farina, F., 2011. The enigmatic sources of I-type granites: the peritectic connexion, Lithos 126, 174-181,
- Curry, A., Gaynor, S.P., Davies, J.H.F.L., Ovtcharova, M., Simpson, G., Caricchi, L., 2021. Timescales and thermal evolution of large silicic magma reservoirs during an ignimbrite flare-up: perspectives from zircon. Contrib. Mineral. Petrol. 176.
- Davis, J., Hawkesworth, C., 1993. The petrogenesis of 30-20 Ma basic and intermediate volcanics from the Mogollon-Datil Volcanic Field, New Mexico, USA, Contrib. Mineral. Petrol. 115, 165-183.
- Eddy, M.P., Bowring, S.A., Miller, R.B., Tepper, J.H., 2016. Rapid assembly and crystallization of a fossil large-volume silicic magma chamber. Geology 44, 331-334.
- Farina, F., Dini, A., Davies, J.H.F.L., Ovtcharova, M., Greber, N.D., Bouvier, A.S., Baumgartner, L., Ulianov, A., Schaltegger, U., 2018. Zircon petrochronology reveals the timescale and mechanism of anatectic magma formation, Earth Planet, Sci. Lett. 495, 213-223.
- Farmer, G.L., Bailley, T., Elkins-Tanton, L.T., 2008. Mantle source volumes and the origin of the mid-Tertiary ignimbrite flare-up in the southern Rocky Mountains, western U.S. Lithos 102, 279-294.
- Gaynor, S.P., Coleman, D.S., Rosera, J.M., Tappa, M.J., 2019. Geochronology of Bouguer gravity low. J. Geophys. Res., Solid Earth 124, 2457-2468.
- Gaynor, S.P., Ruiz, M., Schaltegger, U., 2022a. The importance of high precision in the evaluation of U-Pb zircon age spectra. Chem. Geol. 603, 120913.
- Gaynor, S.P., Svensen, H., Polteau, S., Schaltegger, U., 2022b. Local melt contamination and global climate impacts: dating the emplacement of Karoo LIP sills in organic-rich shale. Earth Planet. Sci. Lett. 579, 117371.
- Glazner, A.F., 2007. Thermal limitations on incorporation of wall rock into magma. Geology 35, 319-322.
- Glazner, A.F., Coleman, D.S., Bartley, J.M., 2008. The tenuous connection between high-silica rhyolites and granodiorite plutons. Geology 36, 183-186.
- Goodge, J., Vervoort, J., 2006. Origin of Mesoproterozoic A-type granites in Laurentia: Hf isotope evidence. Earth Planet. Sci. Lett. 243, 711-731.
- Hawkesworth, C.J., Kemp, A.I.S., 2006. Using hafnium and oxygen isotopes in zircon
- to unravel the record of crustal evolution. Chem. Geol. 226, 144-162. Humphreys, E., Hessler, E., Dueker, K., Farmer, G.L., Erslev, E., Atwater, T., 2003. How
- the Laramide-Age hydration of North American lithosphere by the Farallon slab controlled subsequent activity in the western United States. In: The George A. Thompson Volume: The Lithosphere of Western North America and Its Geophysical Characterization. Int. Geol. Rev. 45, 524-544.
- Johnson, C.M., 1991. Large-scale crust formation and lithosphere modification beneath middle to late Cenozoic calderas and volcanic fields, western North America. J. Geophys. Res. 96, 13485-13507.
- Karakas, O., Wotzlaw, J.F., Guillong, M., Ulmer, P., Brack, P., Economos, R., Bergantz, G.W., Sinigoi, S., Bachman, O., 2019. The pace of crustal-scale magma accretion and differentiation beneath silicic caldera volcanoes. Geology 47, 719-723.
- Karlstrom, K.E., Amato, J.M., Williams, M.L., Heizler, M., Shaw, C.A., Read, A.S., Bauer, P., 2004. Proterozoic tectonic evolution of the New Mexico region: a synthesis. In: Mack, G.H., Giles, K.A. (Eds.), The Geology of New Mexico: A Geologic History. New Mexico Geological Society, pp. 1-34.
- Keller, C.B., Schoene, B., Samperton, K.M., 2018. A stochastic sampling approach to zircon eruption age interpretation. Geochem. Perspect. Lett. 8, 31-35.
- Kinny, R.D., Maas, R., 2003. Lu-Hf and Sm-Nd isotope systems in zircon. Rev. Mineral. Geochem. 53, 327-341.
- Kuiper, K.F., Deino, A., Hilgen, F.J., Krijgsman, W., Renne, P.R., Wijbrans, J.R., 2008. Synchronizing rock clocks of Earth history. Science 320 (5875), 500-504.
- Lawton, T.F., McMillan, N.J., 1999. Arc abandonment as a cause for passive continental rifting: comparison of the Jurassic Mexican Borderland rift and the Cenozoic Rio Grande rift. Geology 27, 779-782.

- McDowell, F.W., McIntosh, W.C., 2012. Timing of intense magmatic episodes in the northern and central Sierra Madre Occidental, western Mexico. Geosphere 8, 1505–1526.
- McIntosh, W.C., Sutter, J.F., Chapin, C.E., Kedzie, L.L., 1990. High-precision ⁴⁰Ar/³⁹Ar sanidine geochronology of ignimbrites in the Mogollon-Datil volcanic field, southwestern New Mexico. Bull. Volcanol. 52, 584–601.
- McIntosh, W.C., Chapin, C.E., Ratté, J.C., Sutter, J.F., 1992. Time-stratigraphic framework for the Eocene-Oligocene Mogollon-Datil volcanic field, southwest New Mexico. GSA Bull. 104, 851–871.
- McMillan, N.J., Dickin, A.P., Hag, D., 2000. Evolution of magma source regions in the Rio Grande rift, southern New Mexico. Geol. Soc. Am. Bull. 112, 287–303.
- Miller, J.S., Matzel, J.E.P., Miller, C.F., Burgess, S.D., Miller, R.B., 2007. Zircon growth and recycling during the assembly of large, composite arc plutons. J. Volcanol. Geotherm. Res. 167, 282–299.
- Morel, M.L.A., Nebel, O., Nebel-Jacobsen, Y.J., Miller, J.S., Vroon, P.Z., 2008. Hafnium isotope characterization of the GJ-1 zircon reference material by solution and laser ablation MC-ICPMS. Chem. Geol. 255, 231–235.
- Nowell, G.M., Kempton, P.D., Noble, S.R., Fitton, J.G., Saunders, A.D., Mahoney, J.J., Taylor, R.N., 1998. High precision Hf isotope measurements of MORB and OIB by thermal ionisation mass spectrometry: insights into the depleted mantle. Chem. Geol. 149, 211–233.
- Osburn, G.R., Chapin, C.E., 1983. Ash-flow tuffs and cauldrons in the northeast Mogollon-Datil volcanic field: a summary. In: New Mexico Geological Society Guidebook, vol. 34, pp. 197–204.
- Pamukçu, A.S., Schoene, B., Deering, C.D., Keller, C.B., Eddy, M.P., 2022. Volcanopluton connections at the Lake City magmatic (Colorado, USA). Geosphere.
- Petford, N., Gallagher, K., 2001. Partial melting of mafic (amphibolitic) lower crust by periodic influx of basaltic magma. Earth Planet. Sci. Lett. 193, 483–489.
- Rioux, M., Farmer, G.L., Bowring, S.A., Wooton, K.M., Amato, J.M., Coleman, D.S., Verplank, P.L., 2016. The link between volcanism and plutonism in epizonal magma systems; high-precision U-Pb zircon geochronology from the Organ Mountains caldera and batholith, New Mexico. Contrib. Mineral. Petrol. 171.
- Rubatto, D., Hermann, J., 2007. Experimental zircon/melt and zircon/garnet trace element partitioning and implications for the geochronology of crustal rocks. Chem. Geol. 241, 38–61.
- Samperton, K.M., Schoene, B., Cottle, J.M., Keller, C.B., Crowley, J.L., Schmitz, M.D., 2015. Magma emplacement, differentiation and cooling in the middle crust: integrated zircon geochronological-geochemical constraints from the Bergell Intrusion, Central Alps. Chem. Geol. 417, 322–340.

- Samperton, K.M., Bell, E.A., Barboni, M., Keller, C.B., Schoene, B., 2017. Zircon agetemperature-compositional spectra in plutonic rocks. Geology 45, 983–986.
- Schaen, A.J., Schoene, B., Dufek, J., Singer, B.S., Eddy, M.P., Jicha, B.R., Cottle, J.M., 2021. Transient rhyolite melt extraction to produce a shallow granitic pluton. Sci. Adv. 7. 11 p.
- Schaltegger, U., Ovtcharova, M., Gaynor, S.P., Schoene, B., Wotzlaw, J., Davies, J.H.F.L., Farina, F., Greber, N., Szymanowskit, D., Chelle-Michou, C., 2021. Long-term repeatability and interlaboratory reproducibility of high-precision ID-TIMS U-Pb geochronology. J. Anal. At. Spectrom. 36, 1466–1477.
- Schoene, B., 2014. 4.10 U-Th-Pb Geochronology. In: Treatise on Geochemistry, vol. 4, pp. 341–378.
- Schöpa, A., Annen, C., 2013. The effects of magma flux variations on the formation and lifetime of large silicic magma chambers. J. Geophys. Res., Solid Earth 118, 926–942
- Sláma, J., Košler, J., Condon, D.J., Crowley, J.L., Gerdes, A., Hanchar, J.M., Horstwood, M.S.A., Morris, G.A., Nasdala, L., Norberg, N., Schaltegger, U., Schoene, B., Tubrett, M.N., Whitehouse, M.J., 2008. Plešovice zircon a new natural reference material for U–Pb and Hf isotopic microanalysis. Chem. Geol. 249, 1–35.
- Sorokin, M.A., Melnik, O.E., Bindeman, I.N., 2022. Modeling of zircon nucleation and growth rates using crystal size distributions in a cooling magmatic intrusion. Earth Planet. Sci. Lett. 577, 117254.
- Szymanowski, D., Ellis, B.S., Wotzlaw, J.F., Bachmann, O., 2019. Maturation and rejuvenation of a silicic magma reservoir: High-resolution chronology of the Kneeling Nun Tuff. Earth Planet. Sci. Lett. 510, 103–115.
- Widmann, P., Davies, J.H.F.L., Schaltegger, U., 2019. Calibrating chemical abrasion: its effects on zircon crystal structure, chemical composition and U-Pb age. Chem. Geol. 511, 1–10.
- Woodhead, J., Hergt, J., Shelley, M., Eggins, S., Kemp, R., 2004. Zircon Hf-isotope analysis with an excimer laser, depth profiling, ablation of complex geometries and concomitant age estimation. Chem. Geol. 209, 121–135.
- Wotzlaw, J.F., Schaltegger, U., Frick, D.A., Dungan, M.A., Gerdes, A., Günther, D., 2013. Tracking the evolution of large-volume silicic magma reservoirs from assembly to supereruption. Geology 41, 867–870.
- Wotzlaw, J.F., Bindeman, I.N., Stern, R.A., D'Abzac, F.X., Schaltegger, U., 2015. Rapid heterogeneous assembly of multiple magma reservoirs prior to Yellowstone supereruptions. Sci. Rep. 5, 14026.